Time-dependent density functional theory with twist-averaged boundary conditions

B. Schuetrumpf, W. Nazarewicz, and P.-G. Reinhard

Phys. Rev. C **93**, 054304 — Published 2 May 2016

DOI: 10.1103/PhysRevC.93.054304

Time-dependent density functional theory with twist-averaged boundary conditions

B. Schuetrumpf
FRIB Laboratory, Michigan State University, East Lansing, Michigan 48824, USA

W. Nazarewicz
Department of Physics and Astronomy and FRIB Laboratory, Michigan State University, East Lansing, Michigan 48824, USA and Faculty of Physics, University of Warsaw, 02-093 Warsaw, Poland

P.-G. Reinhard
Institut für theoretische Physik, Universität Erlangen, D-91054 Erlangen, Germany

Background: Time-dependent density functional theory is widely used to describe excitations of many-fermion systems. In its many applications, 3D coordinate-space representation is used, and infinite-domain calculations are limited to a finite volume represented by a spatial box. For finite quantum systems (atoms, molecules, nuclei, hadrons), the commonly used periodic or reflecting boundary conditions introduce spurious quantization of the continuum states and artificial reflections from boundary; hence, an incorrect treatment of evaporated particles.

Purpose: The finite-volume artifacts for finite systems can be practically cured by invoking an absorbing potential in a certain boundary region sufficiently far from the described system. However, such absorption cannot be applied in the calculations of infinite matter (crystal electrons, quantum fluids, neutron star crust), which suffer from unphysical effects stemming from a finite computational box used. Here, twist-averaged boundary conditions (TABC) have been used successfully to diminish the finite-volume effects. In this work, we extend TABC to time-dependent modes.

Method: We use the 3D time-dependent density functional framework with the Skyrme energy density functional. The practical calculations are carried out for small- and large-amplitude electric dipole and quadrupole oscillations of ^{16}O. We apply and compare three kinds of boundary conditions: periodic, absorbing, and twist-averaged.

Results: Calculations employing absorbing boundary conditions (ABC) and TABC are superior to those based on periodic boundary conditions. For low-energy excitations, TABC and ABC variants yield very similar results. With only four twist phases per spatial direction in TABC, one obtains an excellent reduction of spurious fluctuations. In the nonlinear regime, one has to deal with evaporated particles. In TABC, the floating nucleon gas remains in the box; the amount of nucleons in the gas is found to be roughly the same as the number of absorbed particles in ABC.

Conclusion: We demonstrate that by using TABC, one can reduce finite-volume effects drastically without adding any additional parameters associated with absorption at large distances. Moreover, TABC are an obvious choice for time-dependent calculations for infinite systems. Since TABC calculations for different twists can be performed independently, the method is trivially adapted to parallel computing.

PACS numbers: 02.60.Lj,21.60.Jz,24.30.Cz,31.15.ee

I. INTRODUCTION

The time-dependent density functional theory (TDDFT) for electronic systems had been developed as dynamical extension of stationary DFT [1] in the early 1980ies [2] and has evolved in the meantime to a widely used, efficient, and reliable tool to describe the dynamics of all sorts of electronic systems, see [3, 4] for a review of the basics, and [3, 5–7] for examples of applications. A parallel development took place in nuclear physics where TDDFT is known under the notion of time-dependent Hartree-Fock (TDHF) scheme. TDHF as such was proposed as early as 1930 in [8]. Applications to nuclei started in the mid 1970ies when appropriate computing facilities became available [9–11]. The ever-improving computational capabilities had led to a revival of TDHF without symmetry restrictions, applied to both finite systems [12–16] and infinite matter under astrophysical conditions [17–19]. The numerical tool of choice for truly dynamical processes are coordinate- or momentum-space representations of wave functions and fields and there exists a great variety of published codes using these techniques for electronic systems [20, 21] as well as for nuclear TDHF [22].

A problem pertaining to all numerical solutions of TDDFT is that one is bound to use finite basis sets. For example, the most widely used scheme is based on the coordinate-space representation of wave functions, densities, and potentials. The size of the box, in which computations are carried out, is finite, and this implies that either reflecting or periodic boundary conditions (PBC) are imposed [22]. This leads to unphysical artifacts. One problem is that particles which are in principle emitted from the system and thus traverse the box boundaries are coming back to the system area (reflected or reentering the simulation box from the opposite side) and so perturb the dynamical evolution. Moreover, due to the presence of finite box, the continuum states are artifi-

cially discretized, and this produces artifacts at energies above continuum threshold. Green's functions methods allow to cope with this problem in the regime of linear response [23, 24]. In case of grid representations, one has to work on the boundary conditions. Outgoing, or radiation, boundary conditions which exactly connect the dynamics on the grid to free flow in outer space are proposed as solution [25–27], but they are very elaborate and hard to implement in fully three dimensional grid representations. An efficient and practical method are ABC, which were introduced first in atomic calculations [28, 29] and are meanwhile also used in nuclear TDHF [12, 30, 31]. Although they can be implemented technically with different algorithms, they amount in practice to adding an imaginary potential in a certain boundary region. The quality of the absorption depends on the profile of the imaginary potential and its width [30]. A good working compromise has to be found in each application anew in order to suppress unwanted remaining reflections as much as necessary.

Problems with finite simulation boxes appear also in calculations of infinite matter. Periodic boundary conditions are appropriate in this case, and yet, the wave functions are forced to be strictly periodic which induces spurious quantization effects. This can be avoided by TABC [32–34], often referred to as 'integration over boundary conditions'. According to the Floquet-Bloch theorem, a wave function in a periodic potential is periodic up to a complex phase shift (twist) when going from one cell to the next. Averaging over different phase shifts very efficiently suppresses unwanted spurious quantization effects [35–39]. The benefits of TABC have also been demonstrated in nuclear physics, including time-independent simulations of infinite nucleonic matter [40–45] and lattice QCD [46–51]. All these successful applications of TABC indicate that this method can help with the problem of the unphysically discretized continuum in TDHF calculations of finite nuclei. This is the question, which we aim to investigate in this paper and we do that by comparing the performance of TABC with that of ABC.

TABC is designed to suppress spurious finite-size quantization effects and does that very well. It leaves, however, all particles in the simulation box which means that the gas of emitted particles is still around and may perturb system's dynamics. By employing ABC, one can avoid the gas because the emitted particles are removed efficiently. In the same way ABC help to reduce spurious finite-volume quantization effects. However, imperfect absorption always leaves some quantum beating [30]. Moreover, ABC also absorb the outer tails of bound-state wave functions; hence, a faint background of spurious particle emission is produced (to be avoided by sufficiently large boxes). As no practical prescription is perfect, we have to balance advantages and disadvantages of various ways of implementing boundary conditions.

II. BOUNDARY CONDITIONS

TABC are realized by implementing the Bloch boundary conditions

$$\psi_{\alpha\boldsymbol{\theta}}(\boldsymbol{r}+\boldsymbol{T}_i) = e^{\mathrm{i}\theta_i}\psi_{\alpha\boldsymbol{\theta}}(\boldsymbol{r}), \tag{1}$$

where $\boldsymbol{\theta}$ are three phases or twist angles, $\boldsymbol{T}_i$ ($i \in \{x,y,z\}$) is one of the lattice vectors, $\psi_{\alpha\boldsymbol{\theta}}(\boldsymbol{r})$ is the single-particle wave function characterized by the label α. When employing TABC, one runs separately DFT calculations with different twists $\boldsymbol{\theta}$ and averages the results. This can also be applied to the TDDFT case. An observable to be evaluated is averaged according to

$$\langle\hat{O}(t)\rangle = \frac{1}{8\pi^3}\iiint_0^{2\pi} d^3\boldsymbol{\theta}\,\langle\Psi_{\boldsymbol{\theta}}(t)|\hat{O}|\Psi_{\boldsymbol{\theta}}(t)\rangle. \tag{2}$$

Considering the spatial symmetry of the problem, it is sufficient to average over θ_i between 0 and π in all three directions for the isoscalar E2 mode and in the x and y directions for the isovector E1 mode. The 3D integration over $\boldsymbol{\theta}$ is carried out using an n-point Gauss-Lagrange quadrature between 0 and π and $2n$-point between 0 and 2π. The total number of TABC TDHF calculations to be performed is thus n^3 for the isoscalar E2 mode and $2n^3$ for the isovector E1 mode. The Slater determinants $|\Psi_{\boldsymbol{\theta}}(t)\rangle$ are obtained through independent TDHF calculations with the different sets of twist angles $\boldsymbol{\theta}$.

ABC can be realized by either introducing an imaginary absorbing potential in a boundary zone or by applying a mask function after each TDHF step. Both methods are equivalent and can be mapped into each other [30]. Here we use the mask function $f(r)$. One masking step reads $\psi_\alpha \to \psi_\alpha f(r)$ with $f(r) = 1$ for $r \le L/2 - l_{\mathrm{abs}}$; $f(r) = \cos\left(\frac{\pi}{2}\frac{r-L/2+l_{\mathrm{abs}}}{l_{\mathrm{abs}}}\right)^p$ for $L/2 - l_{\mathrm{abs}} < r \le L/2$; and $f(r) = 0$ for $r > L/2$, where L is the cubic box length and l_{abs} is thickness of the absorbing sphere. Optimal values of p depend on grid spacing and size of time step [30]. Here we use $p = 0.0675$ throughout. We perform the calculations in two different boxes: ($L = 32\,\mathrm{fm}$, $l_{\mathrm{abs}} = 6\,\mathrm{fm}$) or ($L = 40\,\mathrm{fm}$, $l_{\mathrm{abs}} = 10\,\mathrm{fm}$). Mind that the absorbing zone is applied at all sides such that the active zone without absorption has in both cases the same radius of $L - 2l_{\mathrm{abs}} = 20\,\mathrm{fm}$.

III. METHOD

Our calculations are done using the 3D Skyrme-TDHF solver Sky3d which is based on an equidistant, Cartesian 3D grid [22]. We use it with a grid spacing of $\Delta x = 1\,\mathrm{fm}$ and time steps of $0.1\,\mathrm{fm/c}$. We use the Skyrme energy density functional SV-bas [52]. The natural boundary conditions for the plane-wave representation used are PBC. Note that the long range Coulomb force is treated exactly (i.e., yielding non-periodic $1/r$ asymptotics) using a Green's function formalism [53]. Here we have

extended the code to accommodate ABC and TABC. Our benchmarking calculations are performed for electric dipole and quadrupole oscillations of ^{16}O.

The oscillations are generated by an initial boost $\psi_\alpha(\boldsymbol{r}) \rightarrow \psi_\alpha(\boldsymbol{r})\, e^{-i\eta F(\boldsymbol{r})}$ where η is the excitation strength and F is the electric isovector dipole (E1) operator $F_{E1}(\boldsymbol{r}) = -\tau_\alpha x$ or isoscalar quadrupole (E2) operator $F_{E2}(\boldsymbol{r}) = 2z^2 - x^2 - y^2$, where τ_α is 1 for neutrons and -1 for protons [54]. For the calculations at low excitation energy shown in Figs. 1 and 2 we mask the operators with a Woods-Saxon-like form factor $F(\boldsymbol{r}) \rightarrow F(\boldsymbol{r})/\{1 + \exp[(r - r_0)/\Delta r]\}$ to avoid unphysical artifacts near the box boundaries [55]. Here we chose $r_0 = 5\,\mathrm{fm}$ and $\Delta r = 2\,\mathrm{fm}$ throughout. For the calculations at high excitation energies shown in Figs. 3 and 5, following Ref. [22], we replace the coordinates $\boldsymbol{r} = \{x_i\}$ with periodic substitutes $x_i \rightarrow \sin(2\pi x_i/L)$ to make the excitations explicitly periodic. The boost augments the stationary ground-state wave functions with a velocity field which, in turn, drives dynamics. The observable we look at is the emerging time evolution of the multipole moment $\langle F \rangle$, from which we also produce the spectral distribution of the multipole excitation strength, or power spectrum, by the windowed Fourier transform of the time signal [56]. Since the boost parameter η is an auxiliary quantity, in the following discussion we replace it with the excitation energy $E^* = E(\eta) - E(\eta = 0)$, where $E(\eta = 0)$ is the Hartree-Fock ground-state energy.

IV. RESULTS

Figure 1 shows the isoscalar E2 response at the low excitation energy $E^* = 3\,\mathrm{MeV}$. Compared are PBC, ABC and TABC(n) results, where n denotes the number of twists per direction. The time signal in Fig. 1(a) reveals that PBC induce large-amplitude unphysical beating pattern after about 1000 fm/c. The magnitude of these reverberations is as large as half of the maximum amplitude at $t = 0$. The use of ABC completely extinguishes them. While with TABC(2) there are still some small spurious oscillations, with TABC(4) the damping appears almost the same as with ABC. The corresponding strength functions are displayed in Fig. 1(b). The results obtained with PBC exhibit large fluctuations due to the discretized continuum. With only $n = 2$ points in each direction, these oscillations are almost gone in TABC(2). The results in TABC(4) and ABC variants yield smooth quadrupole strength distributions and both curves are practically the same. Since TABC(4) represent a good compromise between feasibility and accuracy, $n = 4$ is therefore chosen for all following calculations.

Although their results look very similar, the mechanism damping the signals are much different in ABC and TABC variants. With ABC, the erratic nucleon gas is removed from the box whenever it encounters the boundaries. In TABC, the gas remains in the box as the particle number is strictly conserved by $\Psi_{\boldsymbol{\theta}}(t)$ and every single

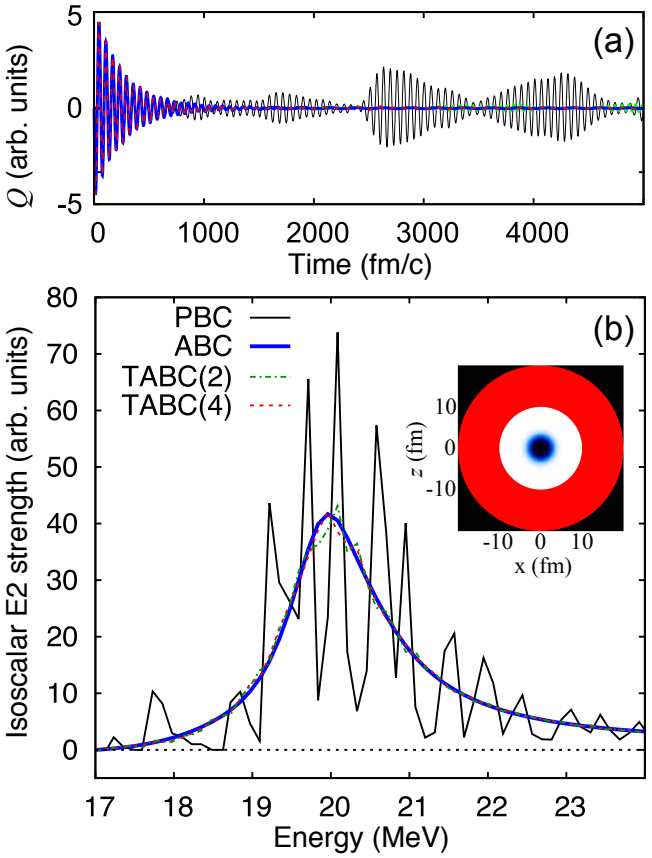

FIG. 1. (Color online) Quadrupole moment $Q(t)$ (a) and strength function (b) for the isoscalar E2 excitation of ^{16}O with $E^* = 3\,\mathrm{MeV}$ and $L = 40\,\mathrm{fm}$. The inset illustrates the geometry of the problem: the total density of ^{16}O (center), the absorption zone (red), and the region of zero density (black). The low-energy part of the spectrum contains very little strength and is not shown.

run for given twist shows qualitatively the same reverberations as PBC. However, these fluctuations enter averaged quantities (2) with different phases and so average out.

We now move to the isovector E1 mode. The corresponding strength function is shown in Fig. 2 for the low excitation energy E^*. To study the dependence of results on box size, we compare results obtained with $L = 32\,\mathrm{fm}$ and $L = 40\,\mathrm{fm}$ by keeping the inner region of ABC (no masking function is applied) the same. The PBC results (not shown) exhibit the spurious finite-volume oscillations, which strongly depends on the box size. As the excitation energy is small, there is a small loss of about 0.1 nucleons in the ABC variant. Overall, ABC and TABC(4) calculations produce fairly similar strength functions for both box sizes. The enhanced shoulder around 24 MeV for $L = 32\,\mathrm{fm}$ in ABC is a faint remainder of the artificial quantization of the continuum [30]. This feature is wiped out by the improved absorption with $L = 40\,\mathrm{fm}$. Another difference appears at the main peak at about 20.5 MeV where both TABC calculations agree

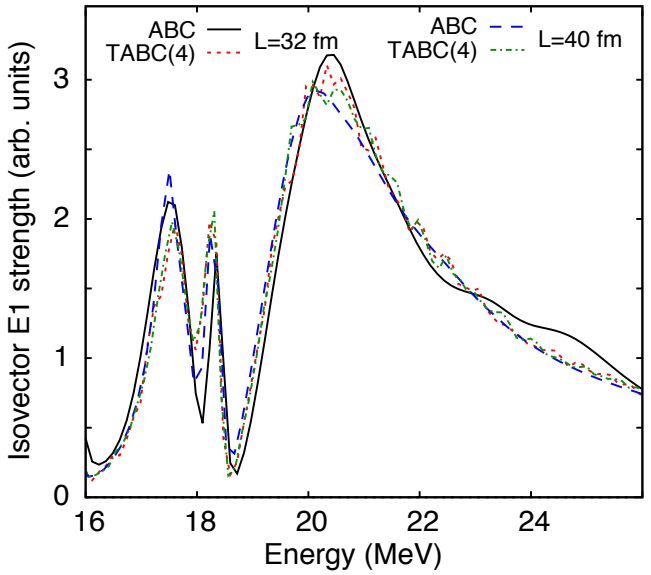

FIG. 2. (Color online) Isovector E1 strength for ^{16}O with $E^* = 1\,$MeV and two box sizes: L=32 and 40 fm.

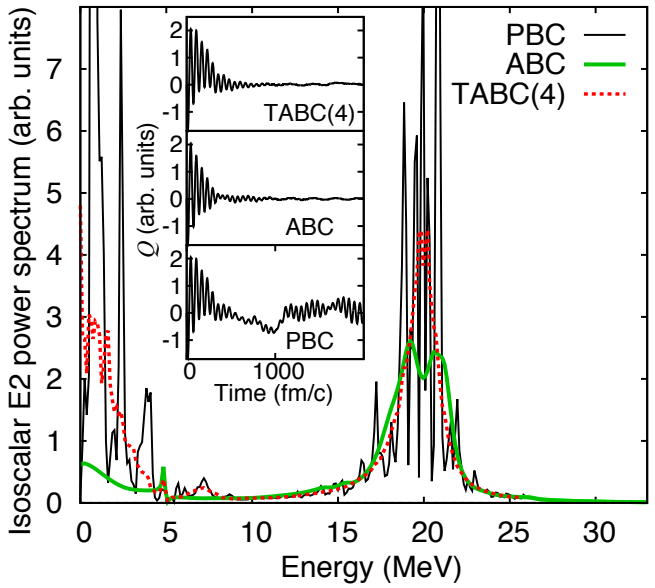

FIG. 3. (Color online) Isoscalar E2 power spectrum for ^{16}O at $E^* = 20\,$MeV and $L = 32\,$fm. The inset shows the time evolution of the mass quadrupole moment Q. See [57] for animations.

aside from small remaining fluctuations which could be further reduced by averaging over more twist points. The maximum for ABC and $L = 40\,$fm appears at a lower energy and is lower as compared to $L = 32\,$fm.

We now proceed to higher excitation energies, $E^* \approx$20 MeV. In this nonlinear regime for ^{16}O [54], we look at the power spectrum. Figure 3 shows results for the isoscalar E2 excitation. In the time signal, PBC shows the pronounced beat pattern stemming from low-frequency oscillations of nucleonic gas moving within the

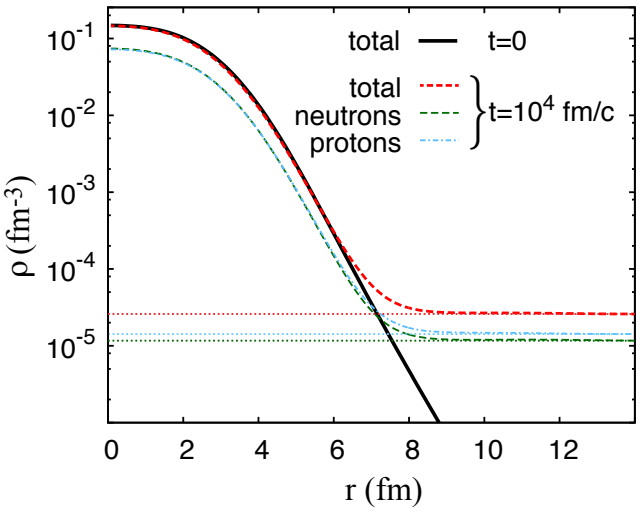

FIG. 4. (Color online) Angular-averaged density distribution corresponding to the isoscalar E2 mode at $E^* = 20\,$MeV at two snapshots: $t = 0$ and $t = 10^4\,$fm/c. The gas densities are indicated by dotted lines: $\rho_{\rm n,gas} = 1.15 \cdot 10^{-5}$fm^{-3} and $\rho_{\rm p,gas} = 1.42 \cdot 10^{-5}$fm^{-3}.

full volume of the box. This effect is well visible in the E2 mode as the quadrupole moment, being quadratic in x, y, and z, is sensitive to the border areas of the box far from the oscillating nucleus. The clouds of oscillating nucleonic gas can be clearly seen in the animations included in Supplemental Material (SM) [57]. Those spurious long-time fluctuations are efficiently wiped out in both ABC and TABC after $t \approx 500\,$fm/c. At shorter times, say the first 200 fm/c, we see some interesting differences in the time signal of TABC and ABC. The initial TABC signal takes a bit longer to decay and the negative amplitudes are suppressed indicating that the evaporated particles are emitted predominantly in the direction of positive quadrupole moment (z-direction). As seen in the animations in SM, the gas particles are absorbed efficiently in ABC, which results in a more symmetric time response.

To understand the effect of the background gas in TABS, Fig. 4 shows angular-averaged density distributions associated with E2 vibrations of Fig. 3. The averaging was done by means of Gaussians centered at mesh points of the original Cartesian 3D grid. At times longer than 500 fm/c, the resulting nucleonic gas is uniformly distributed within the volume of the box. The magnitude of the gas density carries information about the effective temperature of the system and the particle emission rate [58–61]. Integrating the gas density results in 0.38 neutrons and 0.47 protons, and this nicely agrees with the number of absorbed particles in the ABC variant.

The power spectrum for PBC shows large fluctuations in the resonance region around 20 MeV and huge spikes at energies $< 4\,$MeV. Those peaks are removed by ABC and TABC and replaced by smooth low-energy bumps associated with nucleonic gas. In the TABC variant, the number of particles is strictly conserved and the gas is kept

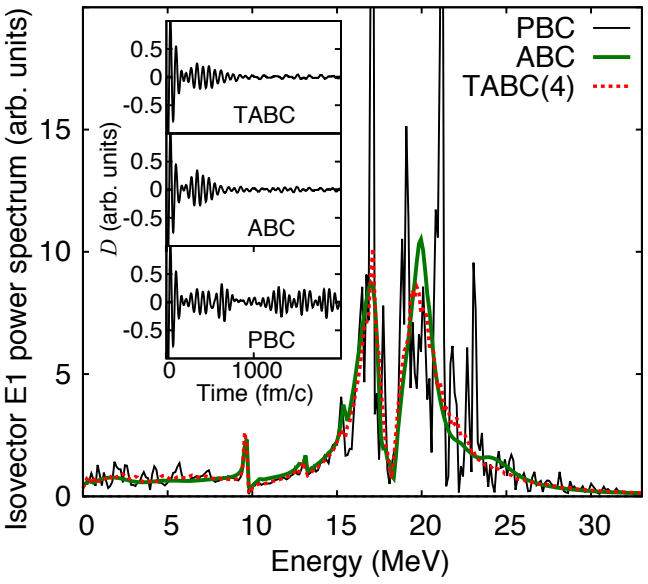

FIG. 5. (Color online) Isovector E1 power spectrum for ^{16}O at $E^* = 22\,\mathrm{MeV}$ and $L = 32\,\mathrm{fm}$. The inset shows the time evolution of the dipole moment D. See [57] for animations.

in the box. This results in a pronounced low-frequency effect. In ABC, absorbing potential removes most of the gas efficiently leaving only the unavoidable effect from a loosely bound nucleon halo. There is also a small difference in the resonance spectra around 20 MeV where a dip appears with ABC. This can be attributed to an effect from the nucleon gas in TABC, which disturbs the dynamics in the resonance region.

The agreement between ABC and TABC is much closer for the E1 mode shown in Fig. 5. We see again that ABC as well as TABC remove the reverberation in the time signal and the spurious fluctuations in the spectrum. Both approaches reproduce nicely the strong enhancement of the low-energy dipole peak at about 10 MeV as well as the flat profile down to $E = 0$.

V. CONCLUSIONS

We demonstrated that TABC can be implemented into TDDFT framework and tested it for nuclear vibrations. Adding no additional parameters, the new approach removes spurious finite-volume effects as efficiently as the previously used method based on ABC. With only two twist phases per direction one obtains a reasonable reduction of spurious fluctuations; four twists per direction offer a good compromise between feasibility and quality. Since TABC calculations for different twists can be performed independently, the method is easily adapted to parallel computing.

For low-energy excitations corresponding to the linear regime, TABC give very similar results as ABC. In the nonlinear regime, ABC absorb noticeable parts of wave functions which for TABC remain in the box as floating nucleon gas. Nonetheless, we see a good agreement. Both methods suppress efficiently the box artifacts and provide very similar spectra, except for some difference in the quadrupole response at very low energies where TABC shows a sizeable bump associated with the slow long-range fluctuations of the nucleon gas. ABC is more efficient in suppressing this artifact.

In future applications, the new TDDFT+TABC method will be applied to excitations of heavy, superfluid nuclei. Furthermore, we intend to apply TABC to infinite systems such as nuclear pasta oscillations in the neutron star crust. In this case, the nucleonic gas represents physical reality, and the low-frequency bump associated with the motion of the cloud within the box is likely to impact the transport properties of the crust.

ACKNOWLEDGMENTS

This material is based upon work supported by the U.S. Department of Energy, Office of Science under Award Numbers DOE-DE-NA0002847 (the Stewardship Science Academic Alliances program) and DE-SC0008511 (NUCLEI SciDAC-3 collaboration). This work used computational resources of the Institute for Cyber-Enabled Research at Michigan State University.

[1] R. M. Dreizler and E. K. U. Gross, *Density Functional Theory: An Approach to the Quantum Many-Body Problem* (Springer-Verlag, Berlin, 1990).
[2] E. Runge and E. K. U. Gross, Phys. Rev. Lett. **52**, 997 (1984).
[3] M. A. L. Marques, C. A. Ullrich, F. Nogueira, A. Rubio, K. Burke, and E. K. U. Gross, eds., *Time-dependent density functional theory*, Lecture Notes in Physics, Vol. 706 (Springer, Berlin, 2006).
[4] E. K. U. Gross, J. F. Dobson, and M. Petersilka, Top. Curr. Chem. **181**, 81 (1996).
[5] P.-G. Reinhard and E. Suraud, *Introduction to Cluster Dynamics* (Wiley, New York, 2004).
[6] F. Furche and K. Burke, Annu. Rep. Comput. Chem., **1**, 19 (2005).
[7] M. Marques and E. Gross, Annu. Rev. Phys. Chem. **55**, 427 (2004).
[8] P. A. M. Dirac, Math. Proc. Cambridge **26**, 376 (1930).
[9] Y. Engel, D. Brink, K. Goeke, S. Krieger, and D. Vautherin, Nucl. Phys. A **249**, 215 (1975).
[10] P. Bonche, S. E. Koonin, and J. W. Negele, Phys. Rev. C **13**, 1226 (1976).
[11] R. Y. Cusson, R. K. Smith, and J. A. Maruhn, Phys. Rev. Lett. **36**, 1166 (1976).

[12] T. Nakatsukasa and K. Yabana, Phys. Rev. C **71**, 024301 (2005).
[13] J. A. Maruhn, P. G. Reinhard, P. D. Stevenson, J. R. Stone, and M. R. Strayer, Phys. Rev. C **71**, 064328 (2005).
[14] A. S. Umar and V. E. Oberacker, Phys. Rev. C **73**, 054607 (2006).
[15] C. Simenel, Eur. Phys. J. A **48**, 152 (2012).
[16] A. S. Umar, V. E. Oberacker, and C. Simenel, Phys. Rev. C **92**, 024621 (2015).
[17] B. Schuetrumpf, K. Iida, J. A. Maruhn, and P.-G. Reinhard, Phys. Rev. C **90**, 055802 (2014).
[18] B. Schuetrumpf, M. A. Klatt, K. Iida, G. E. Schröder-Turk, J. A. Maruhn, K. Mecke, and P.-G. Reinhard, Phys. Rev. C **91**, 025801 (2015).
[19] F. Sébille, V. de la Mota, and S. Figerou, Phys. Rev. C **84**, 055801 (2011).
[20] A. Castro, H. Appel, M. Oliveira, C. A. Rozzi, X. Andrade, F. Lorenzen, M. A. L. Marques, E. K. U. Gross, and A. Rubio, Phys. Stat. Sol. B **243**, 2465 (2006).
[21] P. Giannozzi, S. Baroni, N. Bonini, M. Calandra, R. Car, C. Cavazzoni, D. Ceresoli, G. L. Chiarotti, M. Cococcioni, I. Dabo, A. D. Corso, S. de Gironcoli, S. F., G. Fratesi, R. Gebauer, U. Gerstmann, C. Gougoussis, A. Kokalj, M. Lazzeri, L. Martin-Samos, N. Marzari, F. Mauri, R. Mazzarello, S. Paolini, A. Pasquarello, L. Paulatto, C. Sbraccia, S. Scandolo, G. Sclauzero, A. P. Seitsonen, A. Smogunov, P. U., and R. M. Wentzcovitch, J. Phys. Cond. Mat. **21**, 395502 (2009), arXiv:0906.2569.
[22] J. Maruhn, P.-G. Reinhard, P. Stevenson, and A. Umar, Comput. Phys. Commun. **185**, 2195 (2014).
[23] S. Shlomo and G. F. Bertsch, Nucl. Phys. A **243**, 507 (1975).
[24] G. F. Bertsch and R. A. Broglia, *Oscillations in Finite Quantum Systems*, Cambridge Monographs on Mathematical Physics (Cambridge University Press, Cambridge, 1994).
[25] J. B. Keller and D. Givoli, J. Comput. Phys. **82**, 172 (1989).
[26] K. Boucke, H. Schmitz, and H.-J. Kull, Phys. Rev. A **56**, 763 (1997).
[27] M. Mangin-Brinet, J. Carbonell, and C. Gignoux, Phys. Rev. A **57**, 3245 (1998).
[28] K. C. Kulander, Phys. Rev. A **35**, 445 (1987).
[29] J. L. Krause, K. J. Schafer, and K. C. Kulander, Phys. Rev. A **45**, 4998 (1992).
[30] P.-G. Reinhard, P. D. Stevenson, D. Almehed, J. A. Maruhn, and M. R. Strayer, Phys. Rev. E **73**, 036709 (2006).
[31] C. I. Pardi and P. D. Stevenson, Phys. Rev. C **87**, 014330 (2013).
[32] C. Gros, Z. Phys. B **86**, 359 (1992).
[33] C. Gros, Phys. Rev. B **53**, 6865 (1996).
[34] C. Lin, F. H. Zong, and D. M. Ceperley, Phys. Rev. E **64**, 016702 (2001).
[35] S. Chiesa, D. M. Ceperley, R. M. Martin, and M. Holzmann, Phys. Rev. Lett. **97**, 076404 (2006).
[36] N. Matveeva and S. Giorgini, Phys. Rev. Lett. **109**, 200401 (2012).
[37] L. Shulenburger and T. R. Mattsson, Phys. Rev. B **88**, 245117 (2013).
[38] S. Sorella, Phys. Rev. B **91**, 241116 (2015).
[39] E. Mostaani, N. D. Drummond, and V. I. Fal'ko, Phys. Rev. Lett. **115**, 115501 (2015).
[40] B. Carter, N. Chamel, and P. Haensel, Nuclear Physics A **748**, 675 (2005).
[41] N. Chamel, S. Naimi, E. Khan, and J. Margueron, Phys. Rev. C **75**, 055806 (2007).
[42] S. Gandolfi, A. Y. Illarionov, K. E. Schmidt, F. Pederiva, and S. Fantoni, Phys. Rev. C **79**, 054005 (2009).
[43] F. Gulminelli, T. Furuta, O. Juillet, and C. Leclercq, Phys. Rev. C **84**, 065806 (2011).
[44] G. Hagen, T. Papenbrock, A. Ekström, K. A. Wendt, G. Baardsen, S. Gandolfi, M. Hjorth-Jensen, and C. J. Horowitz, Phys. Rev. C **89**, 014319 (2014).
[45] B. Schuetrumpf and W. Nazarewicz, Phys. Rev. C **92**, 045806 (2015).
[46] P. F. Bedaque and J.-W. Chen, Phys. Lett. B **616**, 208 (2005).
[47] B. C. Tiburzi, Phys. Lett. B **617**, 40 (2005).
[48] V. Bernard, M. Lage, U.-G. Meißner, and A. Rusetsky, J. High Energy Phys. **2011**, 1 (2011).
[49] M. Döring, U.-G. Meißner, and A. Rusetsky, Eur. Phys. J. A **47**, 139 (2011).
[50] R. A. Briceño, Z. Davoudi, T. C. Luu, and M. J. Savage, Phys. Rev. D **89**, 074509 (2014).
[51] R. A. Briceño and M. T. Hansen, Phys. Rev. D **92**, 074509 (2015).
[52] P. Klüpfel, P.-G. Reinhard, T. J. Bürvenich, and J. A. Maruhn, Phys. Rev. C **79**, 034310 (2009).
[53] J. W. Eastwood and D. R. K. Brownrigg, J. Comp. Phys. **32**, 24 (1979).
[54] P.-G. Reinhard, L. Guo, and J. A. Maruhn, Eur. Phys. J. A **32**, 19 (2007).
[55] K. Rutz, J. Maruhn, P.-G. Reinhard, and W. Greiner, Nuclear Physics A **590**, 680 (1995).
[56] F. Calvayrac, E. Suraud, and P.-G. Reinhard, Ann. Phys. (N.Y.) **255**, 125 (1997).
[57] See Supplemental Material at [URL] for animations.
[58] A. K. Kerman and S. Levit, Phys. Rev. C **24**, 1029 (1981).
[59] P. Bonche, S. Levit, and D. Vautherin, Nucl. Phys. A **427**, 278 (1984).
[60] P. Bonche, S. Levit, and D. Vautherin, Nucl. Phys. A **436**, 265 (1985).
[61] Y. Zhu and J. C. Pei, Phys. Rev. C **90**, 054316 (2014).